Highly Efficient Quasi 2D Blue Perovskite Electroluminescence Leveraging a Dual Ligand Composition

Masoud Alahbakhshi, Aditya Mishra, Grigorii Verkhogliadov, Emigdio E. Turner, Ross Haroldson, Austen C. Adams, Qing Gu, Jeffrey J. Rack, Jason D. Slinker, and Anvar A. Zakhidov*

M. Alahbakhshi, Prof. Q. Gu
Department of Electrical and Computer Engineering, The University of Texas at Dallas, 800 West Campbell Road, Richardson, Texas 75080-3021, USA.

A. Mishra, Prof. J. D. Slinker, Prof. A. A. Zakhidov
Department of Materials Science and Engineering, The University of Texas at Dallas, 800 West Campbell Road, Richardson, Texas 75080-3021, USA.
Email: slinker@utdallas.edu

G. Verkhogliadov, Prof. A. A. Zakhidov
ITMO University, School of Physics and Engineering, Kronverkskiy pr. 49, 197101 St. Petersburg, Russia.

G. Verkhogliadov, R. Haroldson, A. C. Adams, Prof. J. D. Slinker, Prof. A. A. Zakhidov
Department of Physics, The University of Texas at Dallas, 800 West Campbell Road, Richardson 75080, USA.

E. E. Turner, Prof J. J. Rack
Department of Chemistry and Chemical Biology, Laboratory for Magneto-Optic Spectroscopy, University of New Mexico, Albuquerque, New Mexico 87131, USA

Prof. J. D. Slinker
Department of Chemistry, The University of Texas at Dallas, 800 West Campbell Road, Richardson 75080-3021, USA.

Prof. A. A. Zakhidov
NanoTech Institute, The University of Texas at Dallas, 800 West Campbell Road, Richardson, Texas 75080-3021, USA.

Keywords: LEDs, perovskite light-emitting diode, perovskite light-emitting electrochemical cell, blue emitter

Perovskite light-emitting diodes (PeLEDs) are advancing because of their superior external quantum efficiencies and color purity. Still, additional work is needed for blue PeLEDs to achieve the same benchmarks as the other visible colors. This work demonstrates an extremely efficient blue PeLED with a 488 nm peak emission, a maximum luminance of 8600 cd m^{-2}, and a maximum external quantum efficiency (EQE) of 12.2% by incorporating the double-sided ethane-1,2-diammonium bromide ($EDBr_2$) ligand salt along with the long-chain ligand

methylphenylammonium chloride (MeCl). The $EDBr_2$ successfully improves the interaction between 2D perovskite layers by reducing the weak Van der Waals interaction and creating a Dion–Jacobson (DJ) structure. Whereas the pristine sample (without $EDBr_2$) is inhibited by small n 2D phases with nonradiative recombination regions that diminish the PeLED performance, adding $EDBr_2$ successfully enables better energy transfer from small n phases to larger n phases. As evidenced by photoluminescence, SEM, and AFM characterization, $EDBr_2$ improves the morphology by reduction of pinholes and passivation of defects, subsequently improving the efficiencies and operational lifetimes of quasi-2D blue PeLEDs.

1. Introduction

Since inception, green, red, and near-infrared perovskite light-emitting diodes (PeLEDs) have rapidly advanced, with external quantum efficiencies (EQEs) increasing from 0.76% to more than 28%,[1] competitive with other LED technologies[2] and indicating a remarkable potential toward practical applications. More recently, blue PeLED performance has also experienced substantial gains but requires additional efforts to reach efficiency similar to the green and red PeLED counterparts. In concert, high-performance RGB color with the precise color purity of perovskite emitters[3] would significantly advance PeLEDs for next-generation optoelectronics, such as displays and light sources. Therefore, there is a vital need to improve blue PeLED performance.[4]

Blue PeLED efficiency has been limited by the instability of the perovskite light-emitting layer and the absence of charge transport materials to reduce the charge injection barrier. So far, many strategies have been proposed and employed to achieve blue PeLEDs.[2-3] The common method utilizes mixed halide 3D perovskite incorporating Cl^- and Br^-, yielding emissions ranging from 450-490 nm.[5] However, mixed halides are subject to irreversible phase separation, and color instability under electrical fields,[6] and halide vacancies cause a reduction of the PLQE of Cl-containing perovskites,[7] though progress in suppressing these deleterious

effects has been shown with blended ionic materials.[5b, 5c] Another method is to form a 2D phase perovskite by inserting large cations and long-chain ligands into a 3D perovskite precursor.[8] Owing to high quantum confinement and strong exciton binding energy, these 2D perovskite structures significantly enhance the perovskite performance.[9] The third method is to synthesize the perovskite nanocrystal structure with strong quantum effects[10], achieved through composition and crystal size modulation. Long-chain organic ligands such as oleic acid (OA) and oleylamine (OLA) are used to passivate the surface defects,[11] and such passivation is crucial to obtaining high-efficiency blue PeLEDs. Generally, quasi-2D perovskites have a fundamental formula of $L_2(ABX_3)_{n-1}BX_4$ (Ruddlesden–Popper phase) or $L(ABX_3)_{n-1}BX_4$ (Dion–Jacobson phase, DJ), where L is an organic ligand cation (such as butylammonium (BA) or phenylethylammonium (PEA)), A stands for monovalent cations (such as Cs^+, MA^+, and FA^+), B is a divalent cation (such as $Pb^{2+}$and Sn^{2+}), X is a smaller halide anion (such as Cl^-, Br^- and I^-) and n represents the number of stacking layers of perovskite crystals. Quasi-2D perovskites are a combination of 2D perovskites with small-n values ($n \leq 2$) and 3D perovskites or 2D perovskites with large-n values.

2D perovskites provide many exceptional opportunities for monitoring material properties and designing applications.[12] Due to the outstanding optoelectronic properties of quasi-2D systems, including large exciton binding energy, high PLQY, energy transfer efficiency, and uniform film formation, there has been extensive and rapid research on quasi-2D blue PeLED structures. Various ideas and strategies, such as quantum-well component modulation (See **Figure S1**, Supporting Information), spacer component modulation for phase redistribution, phase passivation, and electron/hole transport optimization, have been implemented to develop and obtain high-performance blue emission. Yip et al. utilized 2-phenoxyethylamine (POEA) into $MAPbBr_3$ 3D perovskite precursor to fabricate $(POEA)_2(MA)_{n-1}Pb_nB_{r3n+1}$ quasi-2D perovskites LED and successfully shifted the PL and EL spectra from 532 nm (0% POEA) to 480 nm (40% POEA).[8a] Also, Jiang et al. approached a new strategy to tune the “A-site” cation composition

of perovskites to develop blue emitters.[13] In this work, a Rubidium-Cesium alloyed was introduced to form $PEA_2(Rb_xCs_{1-x})_{n-1}Pb_nBr_{3n+1}$ quasi-2D perovskite. This method showed efficient energy transfer from donor domains (low-n) to the emitting domain (high-n) phase, obtaining a PLQY of around 80%. The spectra-stable blue PeLED with a maximum EQE of 1.35%, a half-lifetime of 14.5 min, and a blue spectrum range of 454 to 492 nm was produced.[13] Chu and co-workers introduced a large cation $CH_3CH_2NH_2^+$ (EA^+) into $PEA_2(CsPbBr_3)_2PbBr_4$ perovskite to decrease the Pb–Br orbit coupling and increase the bandgap for blue emission.[14] Replacing Cs^+ with EA^+ cations to form $PEA_2(Cs_{1-x}EA_xPbBr_3)_2PbBr_4$ resulted in a significant increase in PLQY (70%) and achieving 12.1% EQE of sky-blue electroluminescence located at 488 nm.

To obtain efficient quasi-2D blue PeLED, the modulation of the phase distribution by controlling the high n phases and suppressing the low n phases is crucial. Normally, quasi-2D perovskites cover a combination of multi-layered perovskites with small (e.g., n = 1, 2) to large (e.g., n = 4, 5, …) phase distribution. This variance stems from a mixture of colloids with random size distribution in the precursor solution.[15] This phenomenon is particularly important for the small colloids, as filtration usually cannot eliminate them. As a result, they act as the nucleation center in forming the 2D perovskite structure. Nonetheless, the large n (e.g., $n \geq 4$) phases suppress UV emission and induce a spectral red-shifting to the blue region, whereas the formation of small n phases, specifically the n = 1 phase, causes slow energy transfer and severe nonradiative recombination[13, 16]

Extensive research has been done to understand the mechanism of phase modulation. For instance, Xing et al. showed a phase modulation procedure via mixed-ligand $(PEA/IPA)_2A_{n-1}Pb_nBr_{3n+1}$ (IPA = isopropylammonium, A = MA and Cs) quasi-2D perovskite. Increasing the IPA^+/Pb^{2+} ratio suppressed the formation of the small phase (n = 1) and restrained high-n phase development afterward, while the intermediate n phases (n = 2, 3, 4) grew faster than the small n = 1 phase.[16a] This dynamic is significantly helpful in shifting the PL spectrum

toward the blue region (497 nm to 467 nm). As a result, the sky-blue PeLEDs with a maximum luminance of 2480 cd m^{-2} at 490 nm were achieved.

Li and co-workers exhibited a new strategy to modulate the position of the recombination zone by taking advantage of mixed halides of Cl/Br ions were introduced to create $PEA_2Cs_{n-1}Pb_n(Cl_xBr_{1-x})_{3n+1}$ quasi-2D perovskite.[8b] The results showed an efficient energy transfer from the small n values (2D perovskite) to the large n phases (3D perovskite), which in turn yielded an EQE of about 5.7% with a luminance of 3780 cd m^{-2} at an emission peak of 480 nm. Yuan et al. revealed that utilizing the cationic π-conjugated polymer poly [(9,9-bis(3′-((N,N-dimethyl)-N-ethylammonium)-propyl)-2,7-fluorene)-alt-2,7-(9,9-dioctylfluorene)] dibromide (PFNBr) can surprisingly reduce the trap density and in turn, passivate charged ionic defects at grain boundaries.[5a] Sky blue and deeper blue PeLEDs were constructed with EQEs of 11.2% and 8.0% at 485nm and 476nm, respectively. Recently, Zhu and coworkers leveraged 2,2-(ethylenedioxy)bis(ethylammonium) chloride ($EDBECl_2$) to yield a quadi-2D perovskite with a maximum luminance of 2825 cd m^{-2} and a maximum EQE of 13.8%.[17]

Despite extensive progress in perovskite blue emitters, significant challenges remain for these LEDs for large-scale and practical applications. For instance, although high EQE and brightness have been achieved, significant operational stability still needs to be realized. Therefore, we applied a new quasi-2D perovskite composition to achieve high efficiency and increase operational stability. In this work, we developed and optimized a novel dual-ligand composition to generate a reliable and sturdy quasi-2D thin film for efficient blue PeLED application. Applying two ligands into the 3D perovskite precursor can beneficially form small and large n phases. Here, we used $CsPbBr_3$ as the 3D perovskite precursor material, 4-methylphenethylammonium chloride (MeCl) as a long-cation ligand, and ethane-1,2-diammonium bromide ($EDBr_2$) as a second ligand to make the quasi-2D solution. We systematically formed a quantum well structure by optimizing the amount of MeCl and $EDBr_2$ and transferring the energy from low n phases (n = 1) to larger n values (n = 2,3).

2. Quasi-2D Perovskite

2.1. Fabrication Process

First, the $CsPbBr_3$ solution was prepared by dissolving $PbBr_2$ and CsBr in a 1:1.5 molar ratio in anhydrous DMSO. Then the precursor solution was stirred at 60 °C for dissolution overnight. MeCl and $EDBr_2$ (0.5M) were dissolved in DMSO and added to the $CsPbBr_3$ precursor. The $CsPbBr_3$:MeCl solution was optimized by a molar ratio of 0.4:0.2, and then $EDBr_2$ was added in varying percentages x% (x = 2.5, 5, 10, 15 ; x = molarity of $EDBr_2$/molarity of $PbBr_2$). The final solution was kept at room temperature.

Figure 1 schematically shows the in situ fabrication process of quasi-2D thin films. First, the ITO substrates were cleaned. PEDOT:PSS, as an electrode smoothing and work function modifying layer, was spin-coated onto ITO. The substrate was then transferred into a N_2-filled glovebox. Subsequently, the quasi-2D perovskite thin films were prepared carefully in one step spin coating method from precursor solution including $CsPbBr_3$:MeCl:$EDBr_2$ solution. The quasi-2D perovskite precursor solution was then spin-coated at a speed of 2500 rpm for 1 min and annealed at 60 °C for 2 mins. Finally, all samples were transferred to a thermal evaporator. TPBi (40 nm), LiF (1.5 nm), and Al (100 nm) were thermally deposited under vacuum.

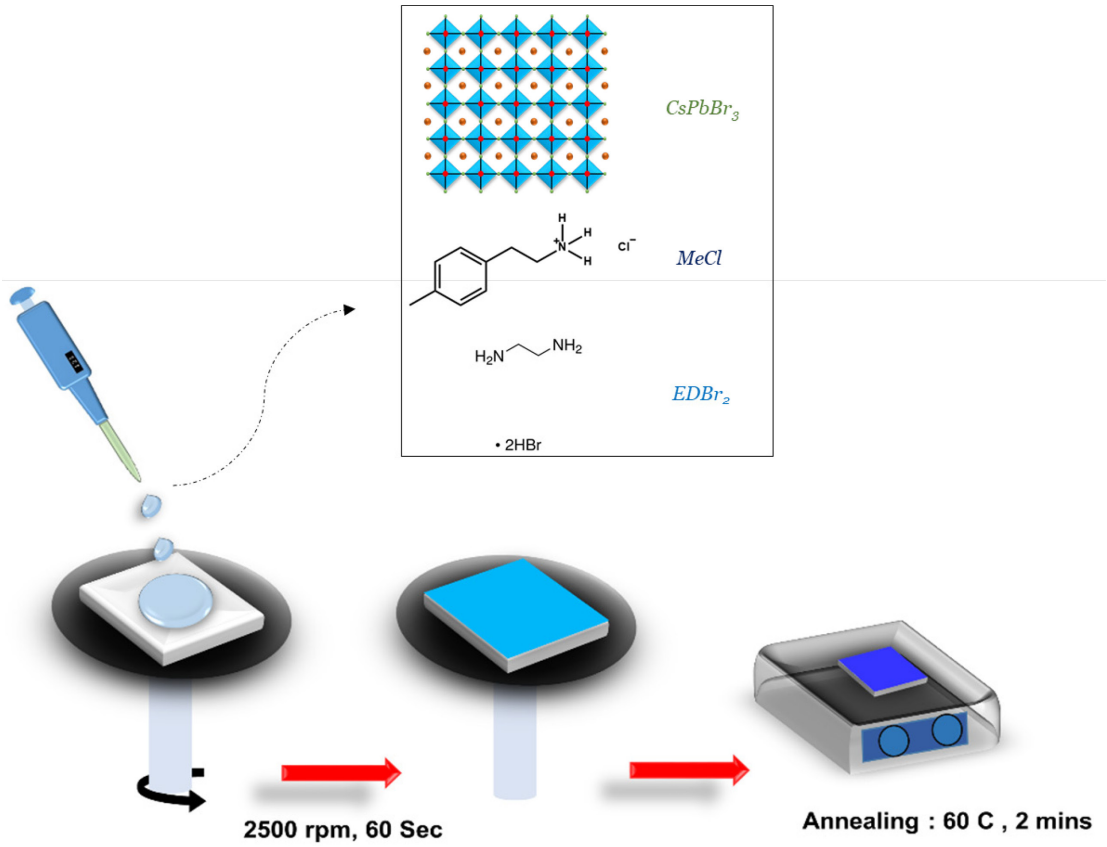

Figure 1. In situ fabrication process of the quasi-2D perovskite thin films.

2.2. Perovskite thin film characterization

To investigate the quasi-2D thin film quality and determine the optimized ratio of $EDBr_2$, UV visible absorption, photoluminescence spectroscopy, scanning electron microscopy (SEM), and X-ray diffraction (XRD) were performed. **Figure 2**b illustrates the absorption spectra of quasi-2D perovskite thin films obtained for different ratios of $EDBr_2$. The excitonic absorption peaks can be identified for the samples derived with different ratio of $EDBr_2$, which appears at ~390, ~418-411, and ~443-437 nm, corresponding to the quantum-well domains with n values of 1, 2, and 3, respectively. With $EDBr_2$ increasing, the excitonic peaks (n = 1) become less recognizable, particularly for 15% $EDBr_2$, implying a reduction of the small n domains and energy transfer from low n phases to large n values. Also, by increasing the amount of $EDBr_2$, n = 2 and n = 3 peaks shift slightly toward the deep blue region. We can ascribe this blue shift

to the fact that the lowest-n and highest-n phases increased slowly, whereas the intermediate n phase (n = 2, 3) grew faster.

X-ray diffraction (XRD) was carried out to understand thin film crystallinity further. According to the XRD patterns in Figure 2a, introducing $EDBr_2$ into the control solution has minimal impact on the crystal structure of the thin films since similar diffraction peaks were observed. However, by increasing the $EDBr_2$ fraction, two peaks at 11.25° and 26.88° emerge, resulting from phase changing from a 3D to a 2D structure.[18] Notably, there is no significant diffraction peak shift, which indicates no formation of hollow perovskite domains or lattice distortion.

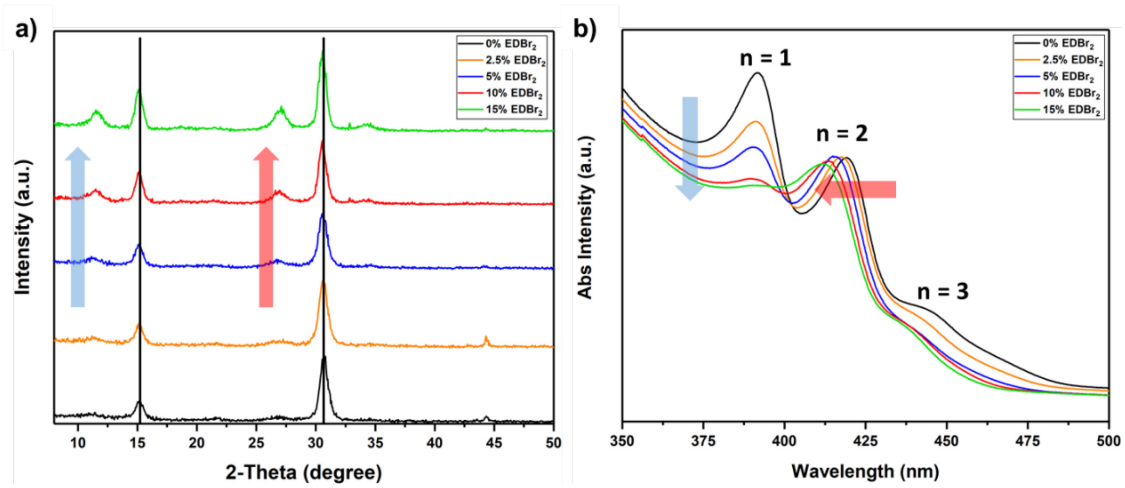

Figure 2. a) The XRD pattern and b) absorption spectra of quasi-2D perovskite thin films incorporating different concentrations of $EDBr_2$.

Perovskite thin films with five different $EDBr_2$ compositions were characterized using femtosecond transient absorption (fs-TA) spectroscopy (**Figure 3** and **Figure S2** and **S3**, Supporting Information). All devices exhibited the following spectral features. Upon excitation, a broad, excited state absorption (ESA) is observed across the entire spectral window. As the experiment progresses, this ESA loses optical density in the red region of the spectrum. The spectral response of each sample also exhibits a bleach feature which contains contributions from both a loss of the ground state (GSB) and emission from excited chromophores. The positions of each of these bleach features are at a longer wavelength than a corresponding peak

in the absorbance spectra, and each bleach has a bandwidth much narrower than in the absorbance spectra. The emission features are red shifted and narrower than their corresponding absorbance transitions because of vibrational cooling processes. Emission occurs from the lowest energy vibrational level in the excited state. In the pristine sample, Figure 3a, there is a large bleach feature at 500 nm, a point at which there is no optical density in the absorbance spectra. These observations imply that these bleach features are predominantly due to emission from the sample and that each emission feature comes from a particular domain number.

A trend is observed in the response of the emission bleach feature across the five samples. The addition of the $EDBr_2$ ligand enhances emission features of the n = 2 and n = 3 domains. When comparing these transient emission features to the steady state emission data shown in **Figure 4**, the n = 3 emission bleach is near the steady state emission peak of the 15% $EDBr_2$ sample. For the pristine sample (Figure 3a), the negative feature is described by discrete and well-resolved negative peaks at 400, 430, 460, and 500 nm. There is a contribution at 475 nm that is obscured by the large bleach feature at 500 nm. Its presence is revealed through kinetic analysis. For 15% $EDBr_2$ (Figure 3e), the bleach features at 400 and 500 nm are diminished, while emission at 430, 460, and 475 nm is emphasized. The wavelengths at which these peaks occur stay consistent from sample to sample—only the relative contribution and bandwidth of each peak change with the addition of $EDBr_2$. This trend follows the change in relative occurrences of domains seen in the absorbance spectra.

All kinetics were fit to a sum of exponentials convolved with a gaussian instrument response function using nonlinear least squares regression analysis. Kinetics were chosen at wavelengths that coincide with either an emission bleach spectral feature or an ESA spectral feature. Complete results of the kinetic fits are given in **Figure S3**, **Equation S1**, and **Table S1-S5**, Supporting Information. In the 15% $EDBr_2$ sample, the emission features required more components to fit, implying additional photophysical processes were introduced. The 475 nm emission bleach is fit with two time components in the 0% $EDBr_2$ sample, 12.7 ± 0.4 ps, and

700 ± 100 ps. The corresponding kinetic in the 15% $EDBr_2$ sample requires three time components, 0.37 ± 0.06 ps, 26 ± 2 ps, and 400 ± 100 ps. The emission feature at 460 nm took two time components in the 0% sample, 6.3 ± 0.2 ps and 250 ± 40 ps, but it required four exponential components in the 15% sample, 0.22 ± 0.04 ps, 6.6 ± 0.5 ps, 43 ± 6 ps, and 1.0 ± 0.3 ns.

The additional fast time components seen in the 15% $EDBr_2$ possess amplitude factors that correspond to growth in the population of the emitting state with time. This is not enough information to determine specific domains contributing to energy transfer. However, it does show that energy transfer into the n=3 domain is occurring. The 460 nm peak is the longest-lived feature in the 15% $EDBr_2$ sample. This corresponds to the steady-state emission peak of the 15% $EDBr_2$ sample. In the 0% $EDBr_2$ sample, the longest-lived feature was the 500nm SE contribution, which does not correspond to the peak of steady-state emission in the sample. A long-lived nonradiative domain in the 0% $EDBr_2$ sample, as is implied by this spectral feature, could cause a decrease in device efficiencies such as those observed comparing these two device types, 0% $EDBr_2$ and 15% $EDBr_2$.

Overall, energy transfer from lower to higher n-domains is enhanced by the inclusion of $EDBr_2$. The inclusion of $EDBr_2$ also increases the lifetime of the n = 3 SE feature while diminishing the lifetimes of the 475 nm and 500nm n>3 SE features. The inclusion of the $EDBr_2$ ligand changes the relative occurrence of each domain and the rates of energy transfer and emission. This is evidenced in the relative contributions of respective emission features in Figure 3 and changes in the absorbance spectra, in Figure 2b. These changes favor emission from the n>3 domain at approximately 460nm. (See **Figure S1**.) Further study of samples with very controlled heterogeneity is needed to isolate and study energy transfer processes between particular domain numbers.

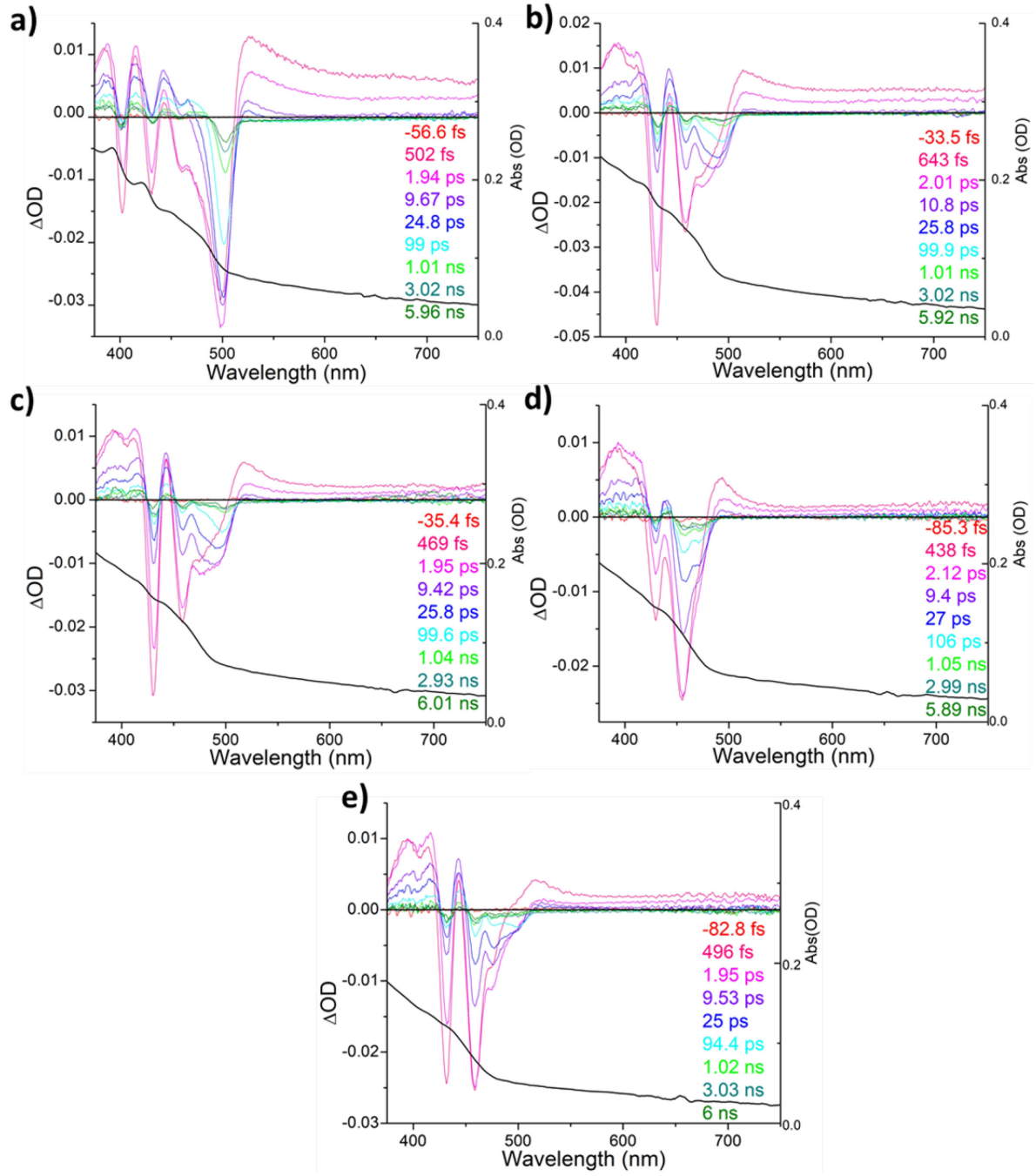

Figure 3. Transient spectroscopy (TA) spectra for quasi-2D perovskite thin films with a) 0%, b) 2.5%, c) 5%, d)10%, and e) 15% $EDBr_2$.

The steady-state photoluminescence stability was carried out to examine the operational stability of thin films under the relatively high excitation power density (CW laser 405 nm, 50 mW cm^{-2}) with different ratios of $EDBr_2$. In Figure 4, the pristine sample (0% $EDBr_2$) shows a 4 nm redshift from 478 to 482 nm after 3 hours of irradiation. However, this redshift was suppressed by adding the $EDBr_2$ ligand into the pristine sample. Regarding the incorporation

of the two different ligands, the pristine sample only includes long-chain MeCl that created a RP quasi-2D structure. This structure has a weak attraction between the 2D layers due to the weak Van der Waals interaction of the methylphenethylammonium ligands that that form a dielectric organic spacer. The low n 2D layers of the pristine perovskite easily dissociates to higher n 2D layers under laser irradiation. However, incorporating the double-sided amino functional group ligand ($EDBr_2$) induces a DJ structure, which has a stronger attraction between 2D layers owing to strong ionic bonding between the PbX_6 octahedron and amino groups of the ligand (Figure 4a and 4b).[19]

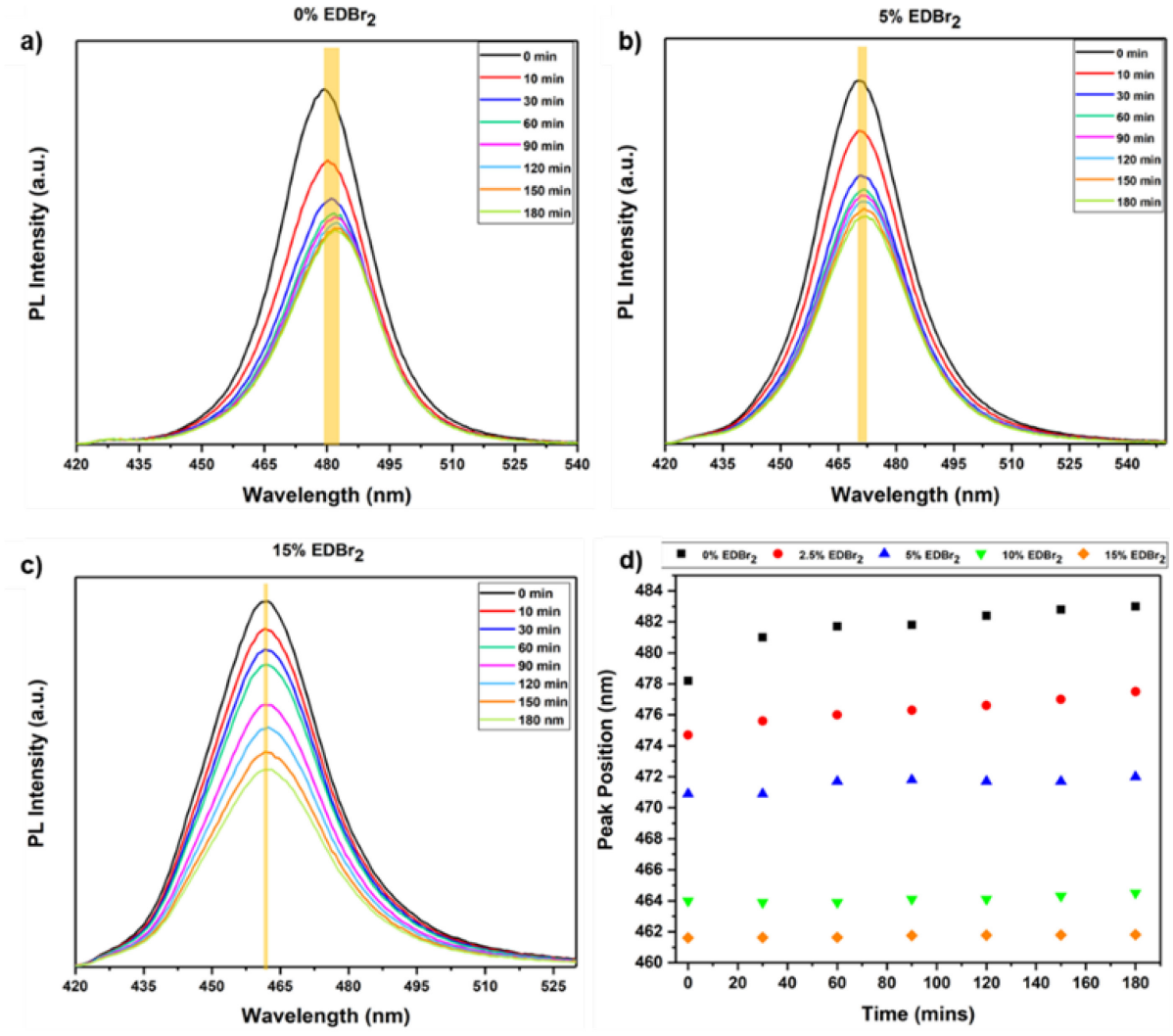

Figure 4. The steady-state photoluminescence stability of quasi-2D perovskite thin films for a) pristine, b) 5%, and c) 15% $EDBr_2$ additive. d) Peak position of PL spectra for different concentrations of $EDBr_2$ additive.

SEM images of quasi-2D thin films (**Figure 5**) show a significant increase in uniformity and reduction of pinholes after introducing $EDBr_2$ into the precursor solution. The precursor thin films (0% $EDBr_2$) exhibit a rough morphology and imperfect surface coverage along with numerous pinholes and defects, resulting in an unstable thin film as noted from the steady-state PL stability (Figure 4). However, after adding $EDBr_2$, the thin films become pinhole-free. In addition, the $EDBr_2$ creates a significant improvement in uniformity and morphology. This is also confirmed by the trend of films under AFM (**Figure S5**, Supporting Information): adding the $EDBR_2$ makes the films smoother and reduces pinholes. The thin film is extremely smooth and uniform for the highest percentage of $EDBr_2$ (15%) due to the high concentration of pure 2D perovskite layers.

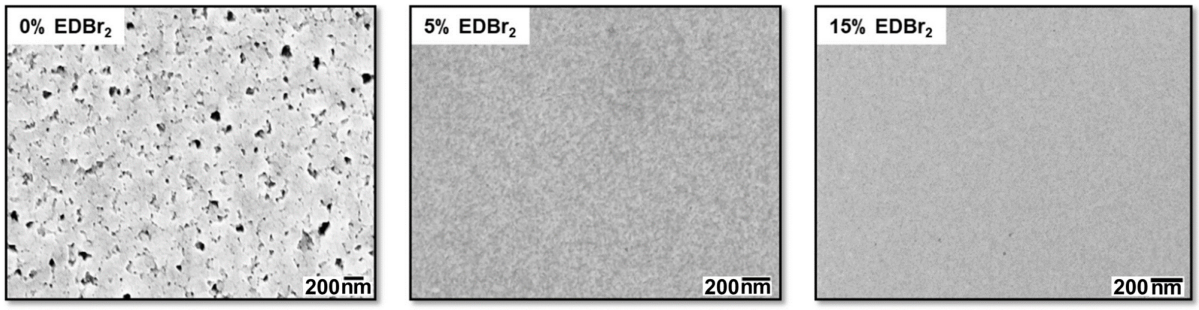

Figure 5. SEM images of quasi-2D perovskite thin films.

3. Quasi-2D Perovskite LEDs

Encouraged by the above studies, we fabricated a blue quasi-2D perovskite LED to realize the impact of $EDBr_2$ on the actual device performance. The device configuration diagram and cross-section SEM image are shown in **Figure 6**, where indium tin oxide (ITO) is the anode, poly(3,4-ethylenedioxythiophene) polystyrene sulfonate (PEDOT:PSS) is the anode modification layer to improve smoothness and achieve work function modification, $CsPbBr_3$:MeCl:$EDBr_2$ (x%) is the emitting layer, 2,2′,2″-(1,3,5-benzinetriyl)-tris(1-phenyl-1-H-benzimidazole) (TPBi) is the electron transport layer (ETL) and lithium fluoride and aluminum (LiF/Al) is the cathode.

The performance of blue PeLED devices is illustrated in **Figure 7**. The current density versus voltage shows a higher value during the J-V measurement for the pristine sample, particularly at lower voltages (>3 V), which is attributed to the higher leakage current due to the poor morphology of the pristine thin film. However, after adding $EDBr_2$, the current density decreases, consistent with fewer pinholes in the films. The maximum luminance increases for all devices with $EDBr_2$ and reaches a maximum of 8600 cd m^{-2} for the 5% $EDBr_2$ sample. The EL spectra peak is located at 488 nm for this 5% $EDBr_2$ device, as seen in **Figure S6** and **S7**, Supporting Information. The CIE plot and coordinates are provided in **Figure S8** and **Table S6**, Supporting Information, respectively, showing the trend toward blue emission with $EDBr_2$ addition. Due to low current density and high luminance, the maximum EQE is increased for all $EDBr_2$ samples and reaches 12.2% for the 5% $EDBr_2$ device (Figure 7b), while the pristine device reaches only 1.8% EQE in the range of current density shown. This enhancement proves that $EDBr_2$ significantly improves the device performance by passivating the traps and defects. This is also evidenced by the notable increase in PLQY of these thin films, ranging from only 5% for the pristine sample to 33% for the $EDBr_2$ (5%) device (Figure 7c). Furthermore, efficient energy transfer from small n phases to large n phases and consequently increasing the radiative recombination in intermediate regions also significantly contribute to the dramatically higher EQE for the $EDBr_2$-treated sample. Further device efficiency metrics and statistics can be found in **Table S7**, Supporting Information. These device enhancements remain robust over repeated measures of individual PeLEDs (n=11), as demonstrated in the histogram of **Figure S9**, Supporting Information, with t-test p-values < 10^{-19} for $EDBr_2$-treated samples relative to untreated samples (**Table S8**, Supporting Information). Regarding the operational lifetime, the EL luminance stability of PeLED was tested by fixing the applied current bias of 0.1 mA (Figure 7d), which produced a maximum luminance of 270 cd m^{-2}. The $EDBr_2$ device shows a luminance half-life (T_{50}) of 160 min, which is higher than most reports (**Table S9**, Supporting

Information). Half-lives were consistent across the various device blends (**Table S10**, Supporting Information).

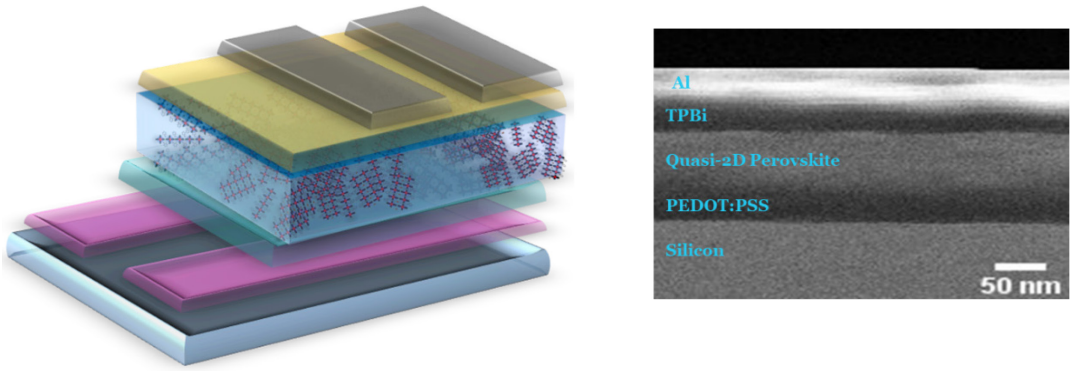

Figure 6. The device structure of blue PeLED and cross-sectional SEM image.

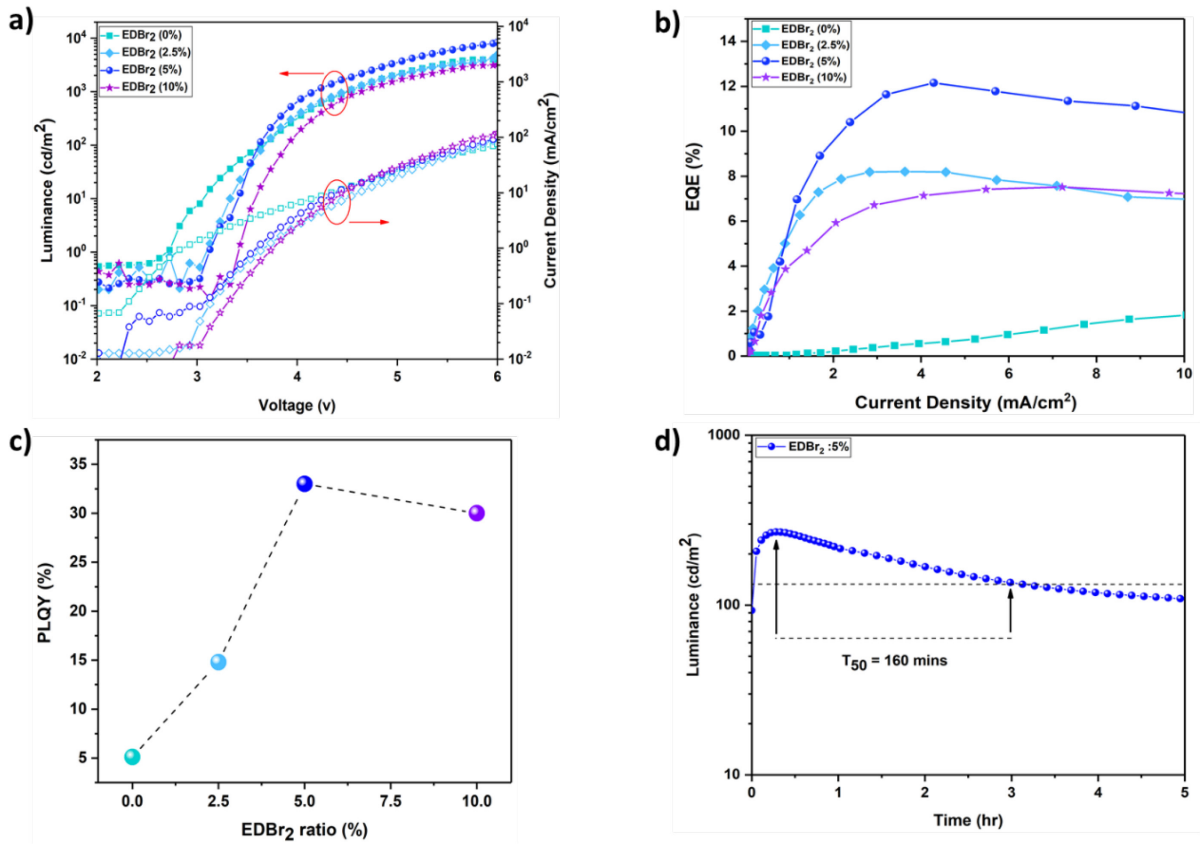

Figure 7. a) Current density and luminance vs. voltage for pristine ($CsPbBr_3$:MeCl) and $EDBr_2$ additive ($CsPbBr_3$:MeCl:$EDBr_2$ (x%)) devices. The inset is an example photo of a device under 5 V operation. b) External quantum efficiency (EQE) of PeLEDs. c) PLQY of quasi-2D thin

films, and d) Operational lifetime of a blue PeLED measured under a constant current of 0.1 mA (Current density 5 mA cm^{-2}).

4. Conclusion

In summary, we demonstrated an extremely efficient blue PeLED with a 488 nm peak emission, a maximum luminance of 8600 cd m^{-2}, and an EQE of 12.2% by utilizing the double-sided amino functional groups of the ethane-1,2-diammonium in $EDBr_2$ and long-chain ligand MeCl. $EDBr_2$ can successfully improve the energy transfer between the 2D perovskite layers by reducing the distance between layers and improving their phase stability via the Dion–Jacobson structure and double ionic bonding instead of the weak Van der Waals interaction between the 2D layers of Ruddleson-Popper perovskite. While the pristine sample (without $EDBr_2$) is dominated by low 2D n phases that have pronounced nonradiative recombination that diminish the PeLED performance, we show that adding $EDBr_2$ successfully enables energy transfer from small n phases to larger n phases. In addition, by performing PL stability, SEM, and AFM characterization, we observe that $EDBr_2$ can improve the morphology by reduction of pinholes and passivation of defects, subsequently improving the efficiencies and operational lifetimes of quasi-2D blue PeLEDs.

5. Experimental Section

Materials: Cesium bromide (CsBr; 99.99%) and polyethylene oxide (PEO; M.W. > 5,000,000) were purchased from Alfa Aesar. Lead (II) bromide ($PbBr_2$; 99.99% trace metal basis), lead (II) chloride ($PbCl_2$; 99.99% trace metal basis), lithium hexafluorophosphate ($LiPF_6$; 99.99%), ethane-1,2-diammonium bromide ($EDBr_2$, >98%), and dimethyl sulfoxide (DMSO; anhydrous > 99.9 %) were purchased from Sigma Aldrich. ITO-coated glass slides were purchased from Thin Film Devices, Inc. (Anaheim, CA). Aluminum (99.99%) was purchased from Kurt J. Lesker. LiF was purchased from Sigma Aldrich.

Quasi 2D perovskite thin film fabrication: First, the $CsPbBr_3$ solution was prepared by dissolving $PbBr_2$ and CsBr in a 1:1.5 molar ratio in anhydrous DMSO. Then the precursor solution was stirred at 60 °C for dissolution overnight. MeCl and $EDBr_2$ (0.5M) were dissolved in DMSO and added to the $CsPbBr_3$ precursor. The $CsPbBr_3$:MeCl solution was optimized by

a molar ratio of 0.4:0.2, and then $EDBr_2$ was added in varying percentages x% (x = 2.5, 5, 10, 15 ; x = molarity of $EDBr_2$/molarity of $PbBr_2$). The final solution was kept at room temperature.

Device fabrication: The ITO/glass substrates (~20 Ω sq^{-1}) were cleaned in a sequence of non-ionic detergent wash, deionized water, acetone, toluene, and 2-propanol in an ultra-sonication bath for 15 mins each. Subsequently, substrates were cleaned in a 20-minute UV ozone treatment. Aqueous poly(3,4-ethylenedioxythiophene):polystyrene sulfonate (PEDOT:PSS) solutions (1.3−1.7%, Clevios AI 4083) were filtered through a 0.45 μm GHP filter and then spin-coated to obtain a ∼20 nm thick film on the ITO-coated glass substrates. These films were subsequently annealed at 125 °C for 10 minutes in a dry N2-filled glovebox. The quasi-2D perovskite precursor solution was then spin-coated at a speed of 2500 rpm for 1 min and annealed at 60 °C for 2 mins. Finally, all samples were transferred to a thermal evaporator. TPBi (40 nm), LiF (1.5 nm), and Al (100 nm) were deposited under a high vacuum of ∼7 $\times 10^{-7}$ torr. The active areas of the devices were 3 mm^2.

Electroluminescence measurements: The current-voltage electrical characteristics were obtained with a 760D electrochemical analyzer from CH Instruments (Austin, TX), with radiant exitance measurements acquired with a calibrated Labsphere integrating sphere equipped with a thermoelectric-cooled silicon photodetector and Keithley 6485 picoammeter. Each cyclic LIV sweep was performed at 0.1V/sec with 5 seconds of interval between each scan. Electroluminescence spectra were measured with an Ocean Optics Jazz fiber spectrometer. Lifetime measurements were obtained with a custom multiplexer testing station capable of measuring 16 light-emitting devices simultaneously. In brief, this instrument supplied constant current and measured voltage with custom circuitry and simultaneously captured radiant flux with a calibrated Hamamatsu photodiode (S2387-1010R) for each device.

Photoluminescence versus time measurements: Measurements were taken using an Ocean Optics QE65000 spectrometer coupled with a fiber optic cable pointed at the thin films through a 425 nm longpass dielectric filter to block out the 405nm CW laser diode excitation signal.

X-Ray Diffraction (XRD): XRD measurements were collected using a Rigaku SmartLab X-ray Cu target (Ka1=1.54059 Å) and a HyPix 3000 detector. The 2-theta/omega scan was consistently performed in the 2-theta range of 10° to 55° with a 0.01° step and a ~1° min^{-1} scan speed.

Transient Absorption and Emission: lifetimes Transient Absorption and Emission lifetimes were collected on an Edinburgh Instruments Lp920 Laser Flash Photolysis Spectrometer. The excitation source consists of a Continuum Surelight Model SLI-10 (Nd:YAG, 10 Hz) with SHG and THG options to generate a 532 nm and 355 nm pump source. A Surelight SSP (dichroic to separate the 532 and 355) is positioned in between the laser and sample to select the pump wavelength. A 450W ozone-free Xe arc lamp is used to generate a microsecond white light supercontinuum probe beam which is arranged in a 90° cross-beam geometry to the incoming laser pulse at the sample. After the sample, the probe beam passes through a monochromator and is captured by a Hamamatsu R928 PMT.

Scanning Electron Microscopy (SEM): Secondary electron SEM images were taken with a Zeiss Supra-40 SEM using an in-lens detector at an accelerating voltage of 10kV.

Atomic Force Microscopy (AFM): The AFM images were performed using a Veeco Nanoscope IV SPM/AFM equipped with a Bruker Nanoscope V Multimode controller box to scrutinize the morphology of thin films. The thin films were scanned over a 3 μm × 3 μm area at a 2 Hz rate using a TAP150A Sb-doped Si AFM tip from Bruker. Tapping mode AFM was used for this characterization. *Statistical Analysis:* Statistical analysis of PeLED EQE was performed and is presented in Table S8, Supporting Information, with a histogram provided in Figure S9, Supporting Information. No pre-processing of data was performed. Data is presented as the mean ± standard deviation for n = 11 devices. A two-tailed t-test was performed with Excel, and p-values were reported.

Data Availability

The data that support the findings of this study are available from the corresponding author upon reasonable request.

Supporting Information
Supporting Information is available from the Wiley Online Library or from the author.

Acknowledgements
A.Z. acknowledges support from the Welch Foundation (AT-1617) and the Russian Science Foundation (19-73-30023). J.D.S. acknowledges support from the National Science Foundation (ECCS 1906505). Q.G. acknowledges support from the Welch Foundation (AT-1992-20190330) and the National Science Foundation CAREER Award (ECCS-1941629).

Received: ((will be filled in by the editorial staff))
Revised: ((will be filled in by the editorial staff))
Published online: ((will be filled in by the editorial staff))

References

[1] a) Z. Chen, Z. Li, T. R. Hopper, A. A. Bakulin, H.-L. Yip, *Rep. Prog. in Phys.* **2021**, *84*, 046401. b) Z. Liu, W. Qiu, X. Peng, G. Sun, X. Liu, D. Liu, Z. Li, F. He, C. Shen, Q. Gu, F. Ma, H.-L. Yip, L. Hou, Z. Qi, S.-J. Su, *Adv. Mater.* **2021**, *33*, 2103268.

[2] K. Zhang, N. Zhu, M. Zhang, L. Wang, J. Xing, *J. Mater. Chem. C* **2021**, *9*, 3795-3799.

[3] a) J. Liang, Y. Du, K. Wang, A. Ren, X. Dong, C. Zhang, J. Tang, Y. Yan, Y. S. Zhao, *Adv. Opt. Mater.* **2022**, *10*, 2101642. b) Z. Wang, F. Wang, B. Zhao, S. Qu, T. Hayat, A. Alsaedi, L. Sui, K. Yuan, J. Zhang, Z. Wei, Z. a. Tan, *J. Phys. Chem. Lett.* **2020**, *11*, 1120-1127. c) Z. Wang, F. Wang, W. Sun, R. Ni, S. Hu, J. Liu, B. Zhang, A. Alsaed, T. Hayat, Z. a. Tan, *Adv. Funct. Mater.* **2018**, *28*, 1804187. d) F. Wang, Z. Wang, W. Sun, Z. Wang, Y. Bai, T. Hayat, A. Alsaedi, Z. a. Tan, *Small* **2020**, 16, 2002940.

[4] Z. Ren, K. Wang, X. W. Sun, W. C. H. Choy, *Adv. Funct. Mater.* **2021**, *31*, 2100516.

[5] a) S. Yuan, L.-S. Cui, L. Dai, Y. Liu, Q.-W. Liu, Y.-Q. Sun, F. Auras, M. Anaya, X. Zheng, E. Ruggeri, Y.-J. Yu, Y.-K. Qu, M. Abdi-Jalebi, O. M. Bakr, Z.-K. Wang, S. D. Stranks, N. C. Greenham, L.-S. Liao, R. H. Friend, *Adv. Mater.* **2021**, *33*, 2103640; b) A. Mishra, M. Alahbakhshi, R. Haroldson, Q. Gu, A. A. Zakhidov, J. D. Slinker, *Adv. Funct.*

Mater. **2021**, *31*, 2102006; c) A. Mishra, M. Alahbakhshi, Q. Gu, A. A. Zakhidov, J. D. Slinker, *ACS Mater. Lett.* **2021**, *3*, 1357-1362.

[6] A. J. Knight, L. M. Herz, *Energy Environ. Sci.* **2020**, *13*, 2024-2046.

[7] X. Zheng, S. Yuan, J. Liu, J. Yin, F. Yuan, W.-S. Shen, K. Yao, M. Wei, C. Zhou, K. Song, B.-B. Zhang, Y. Lin, M. N. Hedhili, N. Wehbe, Y. Han, H.-T. Sun, Z.-H. Lu, T. D. Anthopoulos, O. F. Mohammed, E. H. Sargent, L.-S. Liao, O. M. Bakr, *ACS Energy Lett.* **2020**, *5*, 793-798.

[8] a) Z. Chen, C. Zhang, X.-F. Jiang, M. Liu, R. Xia, T. Shi, D. Chen, Q. Xue, Y.-J. Zhao, S. Su, H.-L. Yip, Y. Cao, *Adv. Mater.* **2017**, *29*, 1603157; b) Z. Li, Z. Chen, Y. Yang, Q. Xue, H.-L. Yip, Y. Cao, *Nat. Commun.* **2019**, *10*, 1027.

[9] a) X. Gong, O. Voznyy, A. Jain, W. Liu, R. Sabatini, Z. Piontkowski, G. Walters, G. Bappi, S. Nokhrin, O. Bushuyev, M. Yuan, R. Comin, D. McCamant, S. O. Kelley, E. H. Sargent, *Nat. Mater.* **2018**, *17*, 550-556; b) J. C. Blancon, A. V. Stier, H. Tsai, W. Nie, C. C. Stoumpos, B. Traoré, L. Pedesseau, M. Kepenekian, F. Katsutani, G. T. Noe, J. Kono, S. Tretiak, S. A. Crooker, C. Katan, M. G. Kanatzidis, J. J. Crochet, J. Even, A. D. Mohite, *Nat. Commun.* **2018**, *9*, 2254.

[10] a) M. C. Weidman, M. Seitz, S. D. Stranks, W. A. Tisdale, *ACS Nano* **2016**, *10*, 7830-7839; b) T. Chiba, S. Ishikawa, J. Sato, Y. Takahashi, H. Ebe, S. Ohisa, J. Kido, *Adv. Opt. Mater.* **2020**, *8*, 2000289; c) F. Yang, H. T. Chen, R. Zhang, X. K. Liu, W. H. Zhang, J. B. Zhang, F. Gao, L. Wang, *Adv. Funct. Mater.* **2020**, *30*, 1908760.

[11] a) G. Almeida, I. Infante, L. Manna, *Science* **2019**, *364*, 833-834; b) J. Ye, M. M. Byranvand, C. O. Martínez, R. L. Z. Hoye, M. Saliba, L. Polavarapu, *Angew. Chem.-Int. Ed.* **2021**, *60*, 21636-21660.

[12] a) S. Parveen, P. K. Giri, *Nanoscale Adv.* **2022**, *4*, 995-1025; b) A. Varghese, Y. Yin, M. Wang, S. Lodha, N. V. Medhekar, *Adv. Mater. Interfaces* **2022**, *9*, 2102174; c) Y.-T. Li, L. Han, H. Liu, K. Sun, D. Luo, X.-L. Guo, D.-L. Yu, T.-L. Ren, *ACS Appl. Electron. Mater.*

2022, *4*, 547-567. d) D. Ghosh, D. Acharya, L. Pedesseau, C. Katan, J. Even, S. Tretiak, A. J. Neukirch, *J. Mater. Chem. A* **2020**, *8*, 22009-22022. e) Z. Ren, J. Yu, Z. Qin, J. Wang, J. Sun, C. C. S. Chan, S. Ding, K. Wang, R. Chen, K. S. Wong, X. Lu, W.-J. Yin, W. C. H. Choy, *Adv. Mater.* **2021**, 33, 2005570.

[13] Y. Jiang, C. Qin, M. Cui, T. He, K. Liu, Y. Huang, M. Luo, L. Zhang, H. Xu, S. Li, J. Wei, Z. Liu, H. Wang, G.-H. Kim, M. Yuan, J. Chen, *Nat. Commun.* **2019**, *10*, 1868.

[14] Z. Chu, Y. Zhao, F. Ma, C.-X. Zhang, H. Deng, F. Gao, Q. Ye, J. Meng, Z. Yin, X. Zhang, J. You, *Nat. Commun.* **2020**, *11*, 4165.

[15] H. Zhao, X. Liu, J. Xu, Z. Li, Y. Fu, H. Zhu, L. Yan, Z. Liu, S. F. Liu, J. Yao, *ACS Appl. Mater. Interfaces* **2020**, *12*, 48756-48764.

[16] a) J. Xing, Y. Zhao, M. Askerka, L. N. Quan, X. Gong, W. Zhao, J. Zhao, H. Tan, G. Long, L. Gao, Z. Yang, O. Voznyy, J. Tang, Z.-H. Lu, Q. Xiong, E. H. Sargent, *Nat. Commun.* **2018**, *9*, 3541; b) D. P. McMeekin, Z. Wang, W. Rehman, F. Pulvirenti, J. B. Patel, N. K. Noel, M. B. Johnston, S. R. Marder, L. M. Herz, H. J. Snaith, *Adv. Mater.* **2017**, *29*, 1607039.

[17] Z. Zhu, Y. Wu, Y. Shen, J. Tan, D. Shen, M.-F. Lo, M. Li, Y. Yuan, J.-X. Tang, W. Zhang, S.-W. Tsang, Z. Guan, C.-S. Lee, *Chem. Mat.* **2021**, *33*, 4154-4162.

[18] a) M. Worku, Q. He, L.-j. Xu, J. Hong, R. X. Yang, L. Z. Tan, B. Ma, *ACS Appl. Mater. Interfaces* **2020**, *12*, 45056-45063; b) Y. Liu, L. K. Ono, G. Tong, H. Zhang, Y. Qi, *ACS Energy Lett.* **2021**, *6*, 908-914.

[19] Y. Shang, Y. Liao, Q. Wei, Z. Wang, B. Xiang, Y. Ke, W. Liu, Z. Ning, *Sci. Adv.* **2019**, *5*, eaaw8072.

Supporting Information

Highly Efficient Quasi 2D Blue Perovskite Electroluminescence Leveraging a Dual Ligand Composition

Masoud Alahbakhshi, Aditya Mishra, Grigorii Verkhogliadov, Emigdio E. Turner, Ross Haroldson, Austen C. Adams, Qing Gu, Jeffrey J. Rack, Jason D. Slinker, and Anvar A. Zakhidov*

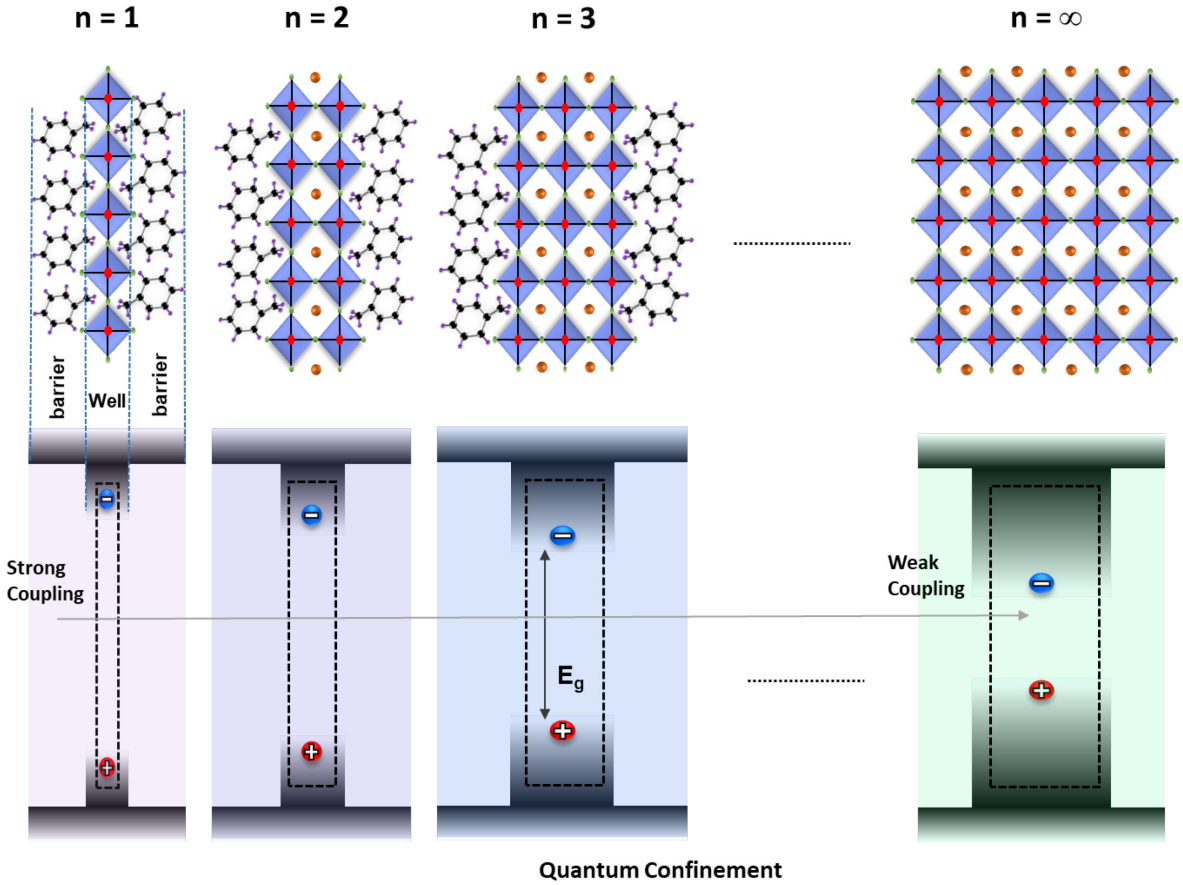

Figure S1. Schematic illustration of quasi-2D perovskites and the energy transfer process.

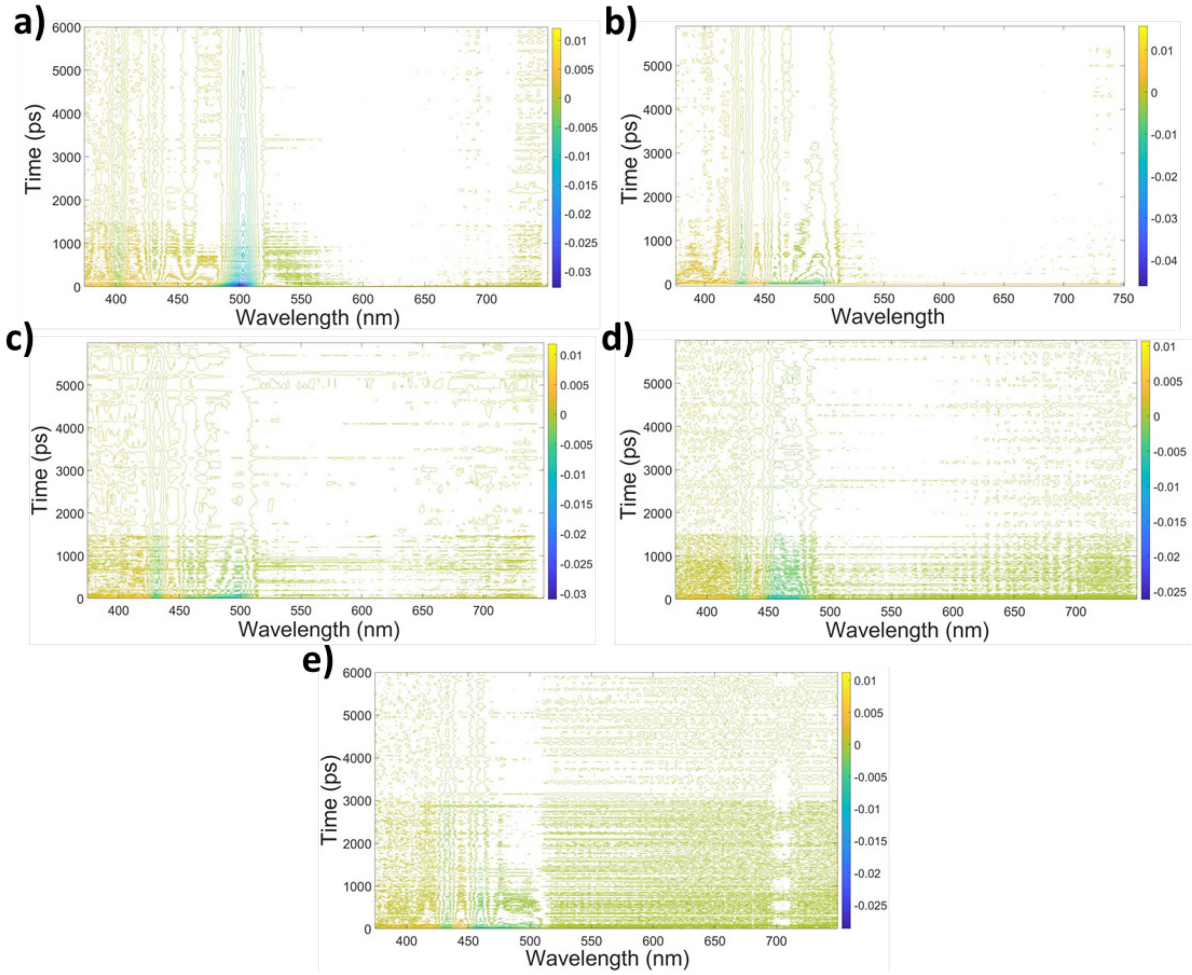

Figure S2. 2D contour plots of quasi-2D perovskite thin films with a) 0%, b) 2.5%, c) 5%, d) 10%, e) 15% $EDBr_2$.

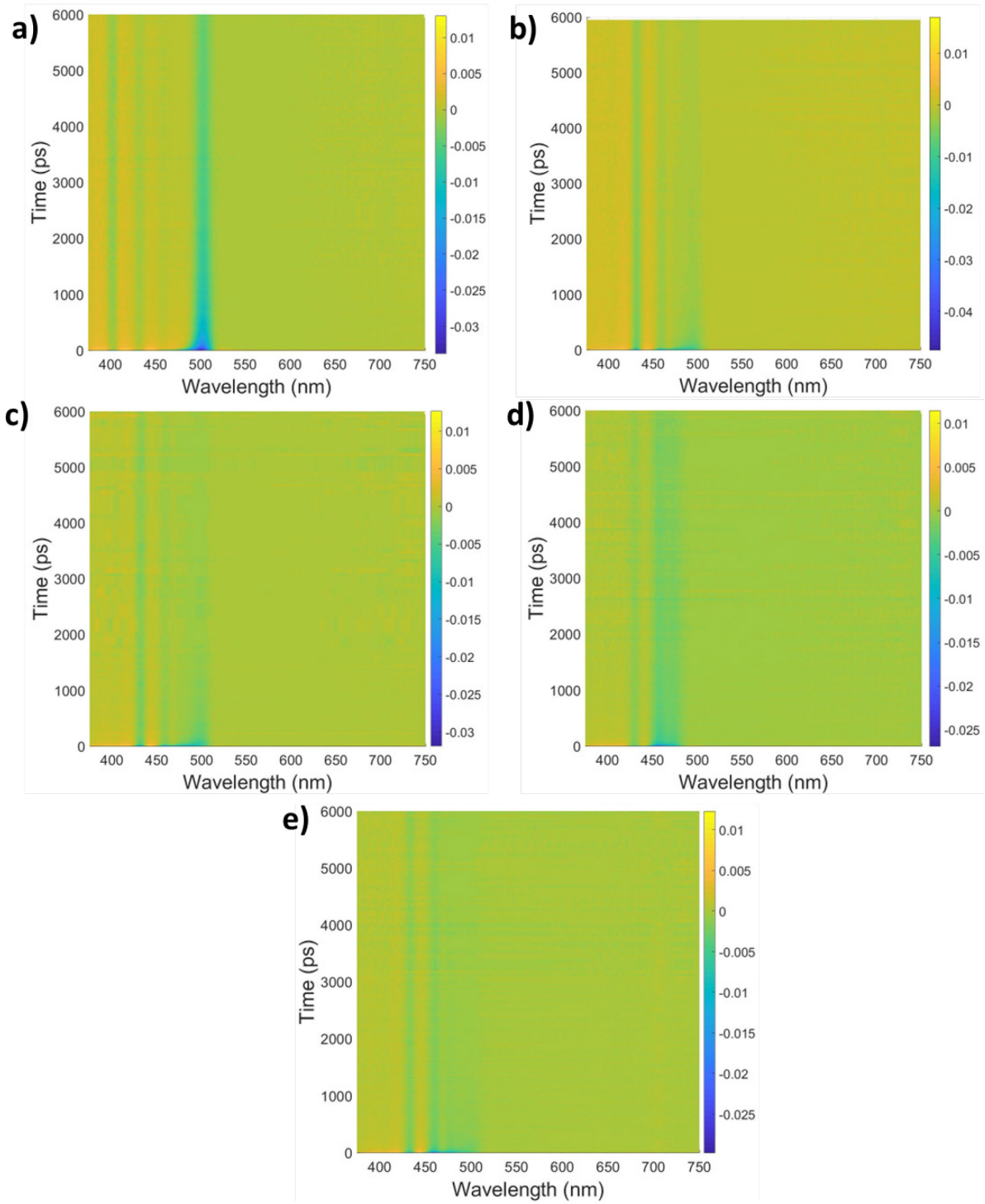

Figure S3. 2D heat map plots of quasi-2D perovskite thin films with a) 0%, b) 2.5%, c) 5%, d) 10%, e) 15% $EDBr_2$.

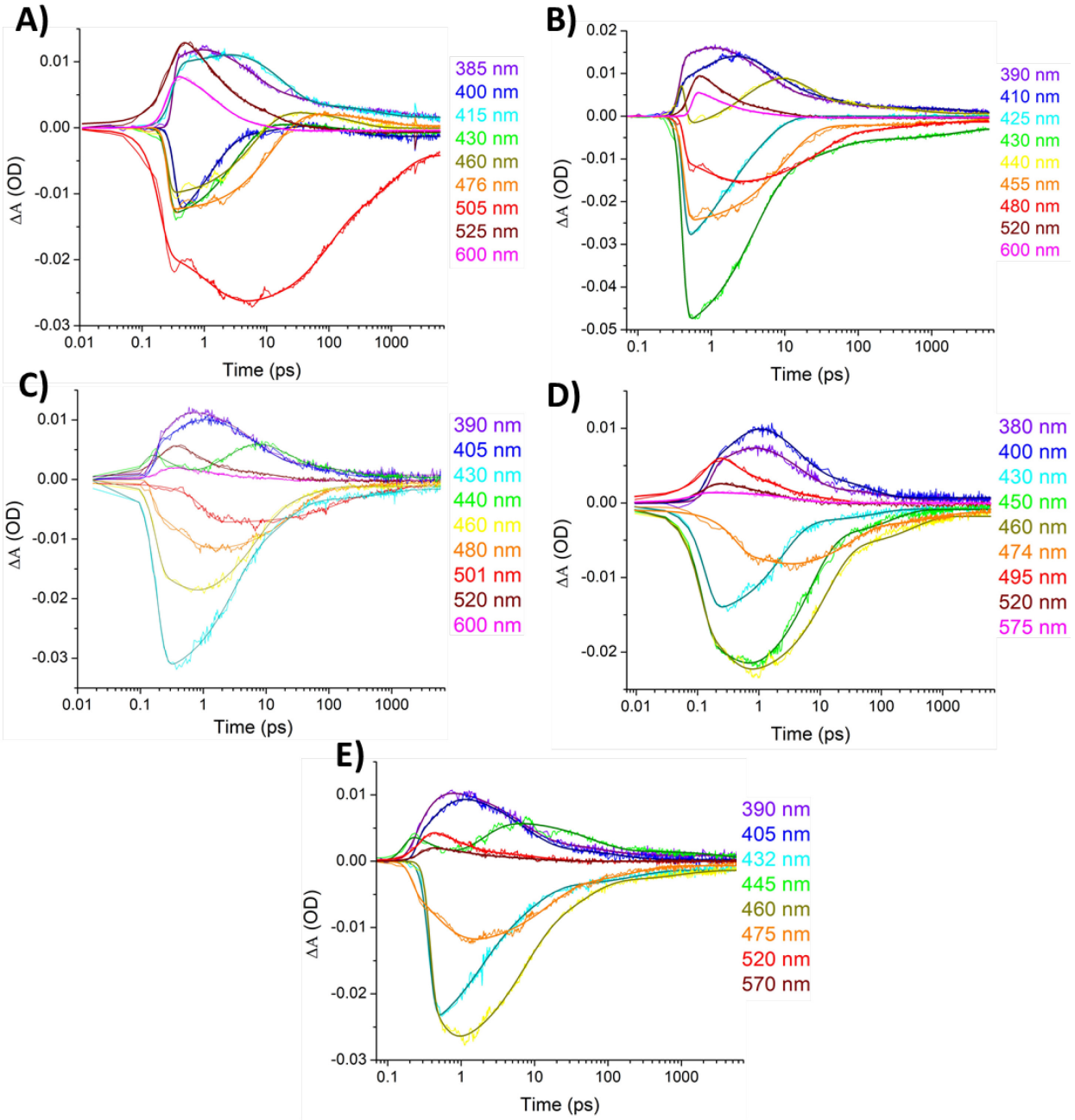

Figure S4. Kinetic traces obtained by transient absorption spectroscopic experiments on A) pristine LED, B) 2.5% $EDBr_2$ LED, C) 5% $EDBr_2$ LED, D) 10%$EDBr_2$ LED, E) 15% $EDBr_2$ LED.

Equation S1. The general form of the equation used to fit the transient absorption kinetic traces

$$y(t) = exp(-(t-t_0)^2 / IRF) * \sum_{n}^{N-1} A_n * exp(-(t-t_0)/\tau_n) + A_N$$

Table S1. Transient Absorption Spectroscopy Kinetic Fit Parameters for pristine LEDs

Wavelength (nm)	385	400	415	430	460	475	505	525	600
t_0 (ps)	0.310	0.325	0.293	0.254	0.249	0.249	0.169	0.236	0.245
±	0.004	0.005	0.007	0.003	0.005	0.003	0.005	0.004	0.003
IRF (ps)	0.070	0.112	0.168	0.089	0.074	0.066	0.141	0.254	0.138
±	0.010	0.012	0.019	0.009	0.013	0.010	0.012	0.010	0.008
A_1 (OD)	-2.79E-	-1.21E-	-3.01E-	-1.40E-	-1.27E-	-1.47E-	8.23E-	9.79E-	6.88E-
±	5.75E-	4.81E-	3.84E-	1.73E-	1.98E-	1.55E-	4.35E-	4.25E-	4.05E-
τ_1 (ps)	0.30	1.19	1.46	3.18	6.28	12.67	1.20	1.13	1.37
±	0.10	0.09	0.36	0.11	0.24	0.41	0.11	0.09	0.11
A_2 (OD)	7.13E-	-2.21E-	9.06E-	1.35E-	2.71E-	1.97E-	-1.25E-	4.97E-	2.21E-
±	4.03E-	4.14E-	3.14E-	1.37E-	1.65E-	1.44E-	4.13E-	4.27E-	4.40E-
τ_2 (ps)	5.87	15.44	18.68	188.40	253.71	693.65	91.01	9.92	8.40
±	0.63	7.78	1.63	48.47	38.49	120.92	5.49	1.84	1.84
A_3 (OD)	2.87E-	2.03E-	2.06E-	-7.00E-	-3.26E-	2.86E-	-1.04E-	1.30E-	-4.30E-
±	4.23E-	2.83E-	1.57E-	5.29E-	7.08E-	1.01E-	3.79E-	3.45E-	1.73E-
τ_3 (ps)	59.28	234.66	618.91				1085.24	91.22	
±	12.86	58.48	99.99				81.46	31.24	
A_4 (OD)	1.42E-	-1.29E-	1.61E-				-4.16E-	-6.20E-	
±	1.43E-	7.03E-	8.53E-				1.70E-	3.03E-	
τ_4 (ps)	1905.99								
±	688.82								
A_5 (OD)	1.50E-								
±	1.70E-								

Table S2. Transient Absorption Spectroscopy Kinetic Fit Parameters for 2.5% $EDBr_2$ LEDs

Wavelength (nm)	390	410	425	430	440	455	480	520	600
t_0 (ps)	0.360	0.356	0.404	0.391	0.364	0.411	0.418	0.498	0.540
±	0.005	0.007	0.002	0.001	0.013	0.005	0.005	0.004	0.005
IRF (ps)	0.099	0.105	0.103	0.113	0.077	0.125	0.083	0.203	0.119
±	0.011	0.018	0.006	0.004	0.115	0.013	0.012	0.011	0.012
A_1 (OD)	-5.29E-	-9.98E-	-1.07E-	-3.59E-	8.16E-02	-2.25E-	6.02E-	8.08E-	4.50E-
±	6.52E-	6.46E-	1.98E-	5.52E-	1.22E+04	2.47E-	3.48E-	3.01E-	3.67E-
τ_1 (ps)	0.39	0.86	1.01	3.80	0.04	9.85	0.75	0.93	0.95
±	0.08	0.11	0.22	0.11	0.01	0.33	0.08	0.08	0.13
A_2 (OD)	1.30E-	1.20E-	-1.91E-	-7.44E-	-1.76E-	-2.18E-	-1.27E-	3.81E-	2.08E-
±	4.37E-	6.96E-	2.20E-	5.87E-	1.09E-03	1.37E-	2.16E-	3.46E-	4.23E-
τ_2 (ps)	5.27	7.04	4.20	38.44	3.63	4134.78	30.21	8.47	6.44
±	0.41	0.82	0.34	4.59	0.26	1019.74	1.51	1.00	1.37
A_3 (OD)	3.60E-	3.99E-		-2.79E-	1.20E-02		-2.43E-	-4.26E-	-3.16E-
±	4.79E-	6.13E-		2.69E-	1.10E-03		2.15E-	2.25E-	1.96E-
τ_3 (ps)	57.79	63.84		2165.34	18.19		587.83		
±	10.99	11.76		684.00	1.91		95.05		
A_4 (OD)	1.22E-	2.09E-		-2.88E-	2.41E-03		-1.32E-		
±	3.74E-	8.21E-		3.30E-	1.68E-04		8.76E-		
τ_4 (ps)	3096.09	7165.83			535.18				
±	2540.92	1207.94			74.23				
A_5 (OD)	7.12E-				6.53E-04				
±	4.59E-				7.83E-05				

Table S3. Transient Absorption Spectroscopy Kinetic Fit Parameters for 5% $EDBr_2$ LEDs

Wavelength (nm)	390	405	430	440	460	480	500	520	600
t_0 (ps)	0.156	0.164	0.166	0.104	0.161	0.153	0.760	0.175	0.184
±	0.021	0.010	0.003	0.009	0.005	0.006	0.030	0.009	0.016
IRF (ps)	0.082	0.061	0.117	0.062	0.100	0.034	1.108	0.204	0.139
±	0.036	0.024	0.008	0.029	0.012	0.015	0.079	0.024	0.044
A_1 (OD)	-6.98E-	-5.80E-	-1.88E-	5.74E-03	5.58E-	6.99E-	-4.02E-	5.37E-	1.56E-
±	2.77E-	8.39E-	1.01E-	6.71E-04	9.77E-	4.97E-	4.44E-	2.91E-	2.74E-
τ_1 (ps)	0.16	0.32	2.74	0.27	0.31	0.37	116.32	0.77	1.18
±	0.05	0.07	0.22	0.06	0.08	0.04	19.38	0.08	0.38
A_2 (OD)	9.06E-	8.17E-	-9.88E-	-9.01E-	-1.52E-	-1.04E-	-2.33E-	1.96E-	7.92E-
±	3.27E-	4.33E-	1.03E-	6.28E-04	8.92E-	2.02E-	4.05E-	1.60E-	2.93E-
τ_2 (ps)	6.68	7.07	19.54	2.79	6.68	28.44	1137.87	18.41	11.81
±	0.55	0.79	3.11	0.47	0.59	1.62	405.61	3.45	6.76
A_3 (OD)	2.36E-	2.80E-	-1.93E-	5.98E-03	-4.36E-	-1.25E-	-8.36E-	-1.96E-	-1.61E-
±	3.01E-	4.25E-	2.64E-	7.35E-04	9.84E-	2.03E-	1.91E-	2.98E-	2.32E-
τ_3 (ps)	147.1	103.1	796.9	19.5	43.0	598.9			
±	38.2	25.1	247.0	3.8	8.7	198.3			
A_4 (OD)	7.79E-	4.20E-	-1.63E-	2.11E-03	-1.15E-	-5.05E-			
±	7.41E-	6.49E-	1.93E-	2.58E-04	5.44E-	1.11E-			
τ_4 (ps)				261.83					
±				53.0565					
A_5 (OD)				0.000425					
±				6.47E-05					

Table S4. Transient Absorption Spectroscopy Kinetic Fit Parameters for 10% $EDBr_2$ LEDs

Wavelength (nm)	380	400	430	450	460	475	495	520	575
t_0 (ps)	0.152	0.135	0.113	0.096	0.086	0.271	0.107	0.107	0.067
±	0.014	0.014	0.005	0.006	0.007	0.026	0.010	0.013	0.018
IRF (ps)	0.089	0.091	0.112	0.103	0.096	0.486	0.159	0.112	0.081
±	0.030	0.031	0.013	0.013	0.014	0.052	0.018	0.034	0.050
A_1 (OD)	-3.73E-	-6.90E-	-1.22E-	6.14E-	8.45E-	2.34E-	4.06E-	1.74E-	1.42E-
±	9.32E-	8.56E-	2.81E-	1.33E-	2.04E-	5.25E-	1.13E-	4.50E-	8.14E-
τ_1 (ps)	0.29	0.37	2.36	0.29	0.21	1.39	0.24	0.87	4.19
±	0.10	0.07	0.15	0.08	0.05	0.50	0.10	0.40	0.59
A_2 (OD)	6.52E-	8.07E-	-1.75E-	-1.93E-	-1.75E-	-5.85E-	3.27E-	1.24E-	-4.80E-
±	3.06E-	4.38E-	2.41E-	3.72E-	2.45E-	2.12E-	3.96E-	5.22E-	2.34E-
τ_2 (ps)	5.02	4.50	81.70	6.77	12.42	32.60	2.06	6.03	
±	0.55	0.59	23.00	0.29	0.47	3.21	0.52	2.68	
A_3 (OD)	1.54E-	3.24E-		-3.72E-	-4.18E-	-1.82E-	1.29E-	-9.70E-	
±	2.58E-	4.22E-		3.05E-	2.06E-	1.76E-	2.40E-	2.57E-	
τ_3 (ps)	110.83	64.22		148.65	332.89	797.71	23.59		
±	34.10	11.38		24.63	37.79	159.75	6.18		
A_4 (OD)	4.94E-	6.93E-		-8.89E-	-1.79E-	-1.27E-	-1.36E-		
±	5.00E-	5.07E-		7.27E-	9.37E-	9.27E-	2.50E-		

Table S5. Transient Absorption Spectroscopy Kinetic Fit Parameters for 15% $EDBr_2$ LEDs

Wavelength (nm)	390	405	430	445	460	470	475	520	570
t_0 (ps)	0.206	0.240	0.355	0.161	0.365	0.227	0.206	0.255	0.265
±	0.072	0.019	0.003	0.012	0.005	0.008	0.015	0.012	0.015
IRF (ps)	0.097	0.069	0.133	0.077	0.111	0.060	0.078	0.186	0.155
±	0.075	0.041	0.009	0.031	0.010	0.019	0.033	0.028	0.039
A_1 (OD)	-9.29E-	-7.40E-	-1.09E-	8.65E-03	8.87E-03	8.35E-03	8.44E-03	3.76E-03	1.37E-03
±	6.53E-03	1.15E-03	1.61E-03	3.74E-03	1.78E-03	6.42E-04	8.48E-04	3.14E-04	2.13E-04
τ_1 (ps)	0.15	0.29	1.50	0.43	0.22	0.32	0.39	0.72	0.85
±	0.04	0.05	0.26	0.16	0.04	0.03	0.05	0.13	0.29
A_2 (OD)	8.16E-03	8.60E-03	-9.91E-	-1.03E-	-1.73E-	-9.62E-	-9.18E-	1.58E-03	9.21E-04
±	3.71E-04	3.07E-04	1.71E-03	3.99E-03	9.50E-04	7.44E-04	2.81E-04	2.21E-04	2.18E-04
τ_2 (ps)	6.45	6.94	8.06	1.38	6.56	8.64	14.93	12.28	9.79
±	0.59	0.55	1.60	0.35	0.50	0.88	1.17	3.25	3.56
A_3 (OD)	2.08E-03	1.84E-03	-2.45E-	4.67E-03	-8.22E-	-3.22E-	-2.93E-	-1.98E-	7.33E-06
±	3.76E-04	2.70E-04	2.25E-04	1.90E-04	9.71E-04	7.83E-04	2.66E-04	2.89E-05	1.95E-05
τ_3 (ps)	94.44	137.30	240.90	61.35	43.07	51.27	218.96		
±	27.15	39.08	47.00	5.37	6.10	12.66	37.43		
A_4 (OD)	8.85E-04	2.60E-04		1.57E-03	-1.67E-	-6.71E-	-6.79E-		
±	5.60E-05	5.90E-05		8.76E-05	2.00E-04	9.44E-05	6.88E-05		
τ_4 (ps)				5924.41	1026.00	2862.97			

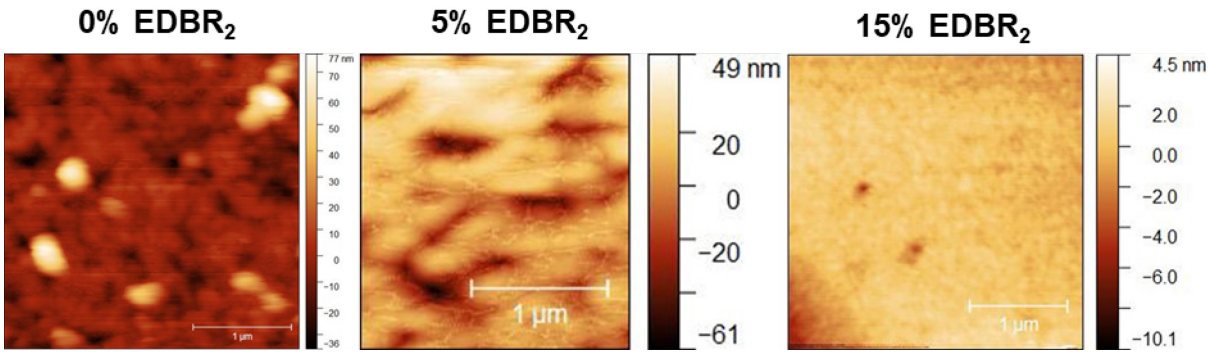

Figure S5. AFM images of quasi-2D perovskite thin films. RMS surface roughnesses were as follows: 0%: 12.2 nm; 5% 17.9 nm; 15% 0.9 nm.

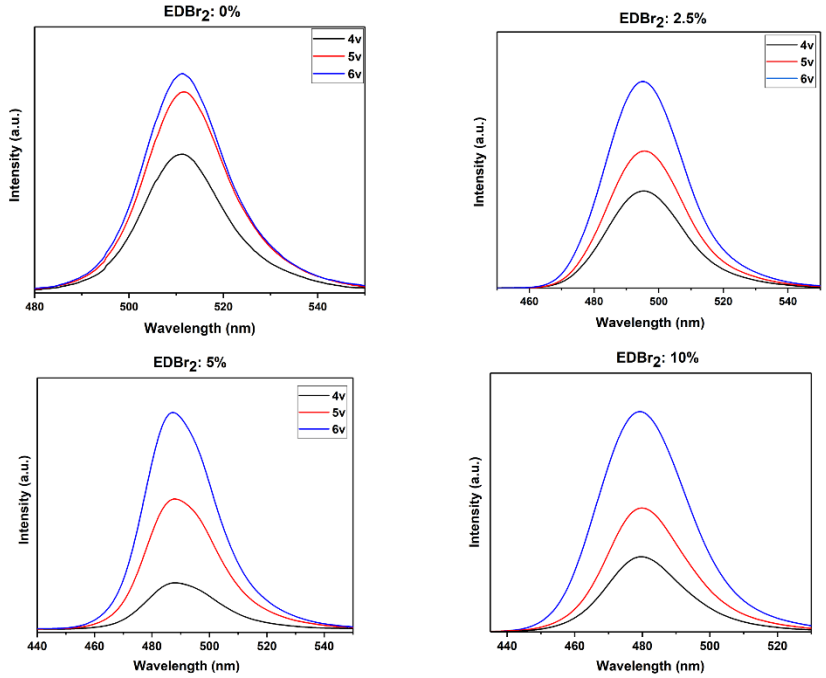

Figure S6. EL spectra and spectral stability of PeLEDs for a) 0%, b) 2.5%, c) 5%, and d) 10% of $EDBr_2$.

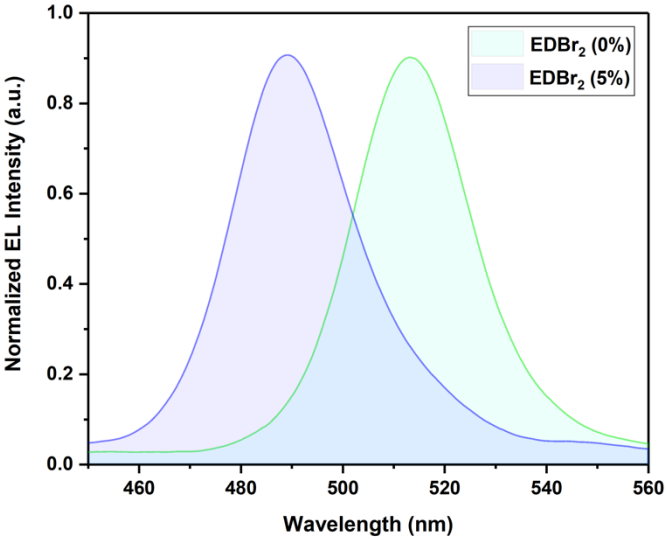

Figure S7. EL spectra of pristine and 5% $EDBr_2$ LEDs.

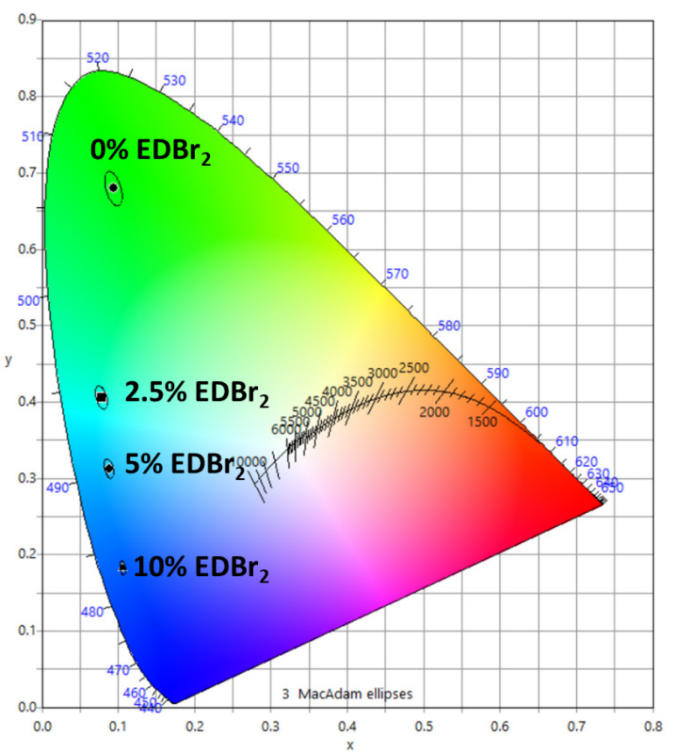

Figure S8. CIE plot for pristine ($CsPbBr_3$:MeCl) and $EDBr_2$ additive ($CsPbBr_3$:MeCl:$EDBr_2$ (x%)) devices.

Table S6. CIE coordinates for pristine ($CsPbBr_3$:MeCl) and $EDBr_2$ additive ($CsPbBr_3$:MeCl:$EDBr_2$ (x%)) devices.

$EDBr_2$ %	0	2.5	5	10
CIE x	0.094	0.078	0.088	0.106
CIE y	0.679	0.406	0.313	0.182

Table S7: Summarized maximum metrics and turn-on voltages for PeLEDs with various fractions of $EDBr_2$.

Sample	Radiant Flux ($\mu W\ m^{-2}$)	Luminace ($cd\ m^{-2}$)	Cur. Eff. ($cd\ A^{-1}$)	Pow. Eff. ($lm\ W^{-1}$)	Ext. QE (%)	Turn-on Voltage (V)
0% $EDBr_2$	82 ± 17	3600 ± 800	6.7 ± 1.2	4.2 ± 0.7	2.0 ± 0.4	2.7
2.5% $EDBr_2$	230 ± 10	5200 ± 300	14 ± 1	12 ± 1	8.1 ± 0.4	3.0
5% $EDBr_2$	490 ± 10	8600 ± 300	17 ± 1	13 ± 1	11.9 ± 0.7	3.1
10% $EDBr_2$	270 ± 20	3400 ± 200	7.5 ± 0.3	5.6 ± 0.2	7.5 ± 0.3	3.3

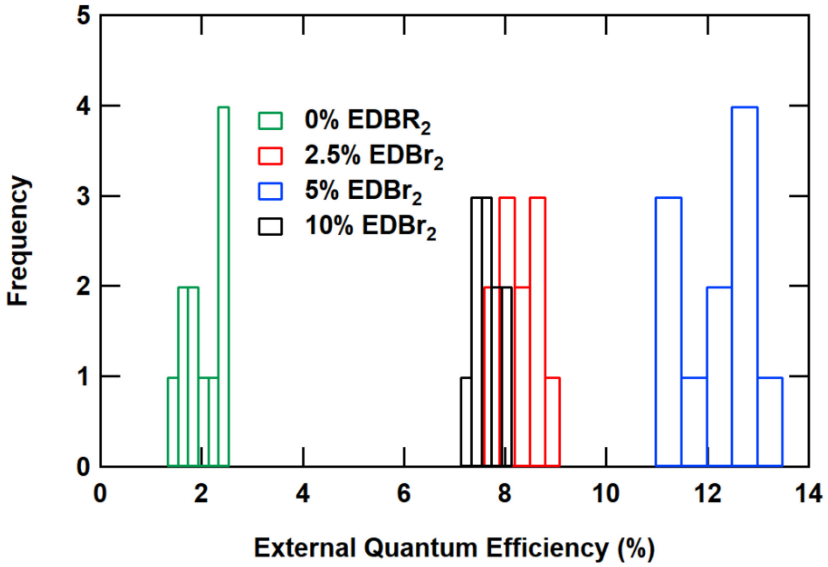

Figure S9. Histogram for n=11 pristine ($CsPbBr_3$:MeCl) and $EDBr_2$ additive ($CsPbBr_3$:MeCl:$EDBr_2$ (x%)) devices. T-test p-values were < 10^{-19} for $EDBr_2$-treated samples relative to pristine samples (**Table S8**, Supporting Information).

Table S8: Summary data for the maximum EQE values for n=11 PeLEDs with various fractions of $EDBr_2$. The P values of the t-tests are low, demonstrating that the $EDBr_2$ device performance has high statistical independence from the pristine devices.

0% $EDBr_2$	2.5% $EDBr_2$	5% $EDBr_2$	10% $EDBr_2$
1.45	7.50	10.86	7.14
1.60	7.52	10.91	7.21
1.69	7.77	11.10	7.32
1.81	7.88	11.51	7.38
1.84	7.98	11.83	7.43
2.02	8.20	12.16	7.52
2.26	8.26	12.25	7.58
2.39	8.39	12.34	7.66
2.40	8.46	12.48	7.74
2.42	8.53	12.66	7.86
2.47	8.73	12.85	8.00
t-test p-values:	9.6E-20	9.7E-21	1.6E-20

Table S9: Comparative performances of the best-in-class quasi-2d blue perovskite LEDs. (The reference list is at the end of the document.)

Perovskites	Device structure	EL Peak [nm]	Luminance [cd m^{-2}]	EQE [%]	T_{50} stability	Yr	Ref
$(PA)_2Cs_{n-1}Pb_nBr_{3n+1}$	ITO/NiOx-PSSNa/perov/TPBi/LiF/Al	492	5737	1.45	220 min@150 cd m^{-2}	2019	[1]
$PEACl:YCl_3:CsPbBr_3$	ITO/PEDOT/Pero/TPBi/LiF/Al	485	9040	11.0	100 min@100 cd m^{-2}	2019	[2]
$PEABr:FA_{0.3}Cs_{0.7}PbBr_3$	ITO/NiOx/TFB/PVK/Perovskite/TPBi/LiF/Al	483	54	9.5	4 min@100 cd m^{-2}	2019	[3]
$PEA_2Cs_{1.6}MA_{0.4}Pb_3Br_{10}$	ITO/PEDOT/TFB/Pero/TPBi/LiF/Al	479	468	5.2	90 min @ 100 cd m^{-2}	2020	[4]
$Na/PEA_2Cs_{n-1}Pb_n(Cl_xBr_{1-x})_{3n+1}$	ITO/NiO_x/PTAA/PVK/Pero/TPBi/LiF/Al	488	2060	11.7	970 s @100 cd m^{-2}	2020	[5]
$PEA_2(Cs_{1-x}EA_xPbBr_3)_2PbBr_4$	ITO/PEDOT/Pero/TPBi/LiF/Al	488 495	2191 2790	12.1 13.3	200s @100 cd m^{-2}	2020	[6]
$(ABA/PEA)_xPA_{2-x}(CsPbBr_3)_{n-1}PbBr_4$	ITO/PVK/Pero/TPBi/LiF/Al	486	513	10.11	81.3 min	2021	[7]
$PEACl:CsPbBr_3:YCl_3$	PEN/ITO/PEDOT/Pero/TPBi/LiF/Al	493	6600	12.8	-	2021	[8]
PEACl:CsPbBr3: ODEA: CsAc	ITO/PEDOT:PSS/PVK/PFI/pero/POT2T/LiF/ Al	483	975	11	171s @100 cd m^{-2}	2022	[9]
Our work: $MeCl:CsPbBr_3:EDBr_2$	ITO/PEDOT/Pero/TPBi/LiF/Al	488	8600	12.2	160 mins @ 270 cd m^{-2}	2022	

Table S10. Luminance half-life at 0.3 mA (15mA cm^{-2}) for PeLEDs with various fractions of $EDBr_2$.

$EDBr_2$ %	0	2.5	5	10
HalfLife (min)	171	185	167	194

References

[1] Z. Ren *et al.*, "Hole Transport Bilayer Structure for Quasi-2D Perovskite Based Blue Light-Emitting Diodes with High Brightness and Good Spectral Stability," *Adv. Funct. Mater.*, vol. 29, no. 43, p. 1905339, Oct. 2019.
[2] Q. Wang *et al.*, "Efficient sky-blue perovskite light-emitting diodes via photoluminescence enhancement," *Nat. Commun.*, vol. 10, no. 1, p. 5633, 2019.
[3] Y. Liu *et al.*, "Efficient blue light-emitting diodes based on quantum-confined bromide perovskite nanostructures," *Nat. Photonics*, vol. 13, no. 11, pp. 760–764, 2019.
[4] D. Ma *et al.*, "Chloride Insertion–Immobilization Enables Bright, Narrowband, and Stable Blue-Emitting Perovskite Diodes," *J. Am. Chem. Soc.*, vol. 142, no. 11, pp. 5126–5134, Mar. 2020.
[5] P. Pang *et al.*, "Rearranging Low-Dimensional Phase Distribution of Quasi-2D Perovskites for Efficient Sky-Blue Perovskite Light-Emitting Diodes," *ACS Nano*, vol. 14, no. 9, pp. 11420–11430, Sep. 2020.
[6] Z. Chu *et al.*, "Large cation ethylammonium incorporated perovskite for efficient and spectra stable blue light-emitting diodes," *Nat. Commun.*, vol. 11, no. 1, p. 4165, 2020.
[7] Z. Ren *et al.*, "High-Performance Blue Perovskite Light-Emitting Diodes Enabled by Efficient Energy Transfer between Coupled Quasi-2D Perovskite Layers," *Adv. Mater.*, vol. 33, no. 1, p. 2005570, Jan. 2021.
[8] Y. Liu *et al.*, "Boosting the efficiency of quasi-2D perovskites light-emitting diodes by using encapsulation growth method," *Nano Energy*, vol. 80, p. 105511, 2021.
[9] Z. Guan *et al.*, "High-Efficiency Blue Perovskite Light-Emitting Diodes with Improved Photoluminescence Quantum Yield via Reducing Trap-Induced Recombination and Exciton–Exciton Annihilation," *Adv. Funct. Mater.*, p. 2203962, Jul. 2022.